Structures and Thermodynamics of Nondilute Polymer Solutions Confined between Parallel Plates

Yongmei Wang*

Department of Chemistry, North Carolina A & T State University, Greensboro, North Carolina 27411

Iwao Teraoka

Department of Chemical Engineering, Chemistry and Materials Science, Polytechnic University, 333 Jay Street, Brooklyn, New York 11201

Received November 2, 1999; Revised Manuscript Received February 22, 2000

ABSTRACT: Lattice Monte Carlo simulations were conducted to study the thermodynamics and structures of linear chain molecules in solutions confined between two parallel plates of various widths over a wide range of concentrations. The results for the chemical potentials, anisotropic chain dimensions, and scattering structure factors are shown and compared with the scaling-law predictions by Daoud and de Gennes [*J. Phys.* (*Paris*) **1977**, *38*, 85]. The transition from a 3D-like solution to a 2D-like solution is observed in both dilute and semidilute regions when the confinement strength increases. In the dilute solution limit, the transition is characterized by an expansion in the chain dimension along the slit walls. In the semidilute region, the transition from 2D dilute pancakes to 2D semidilute pancakes and finally to 3D semidilute spheres with increasing concentration is observed in the dependence of the chain dimension on the concentration. This transition, however, is not clearly seen in the chemical potentials. The single chain structure factors of the confined chains exhibit 2D characteristics in the dilute solution with strong confinement but approach the Debye function in the 2D semidilute and 3D semidilute solutions.

Introduction

Understanding the thermodynamics of nondilute polymer solutions in small confined spaces is important in applications that take advantage of the equilibria of the confined solutions with the surrounding bulk solutions. They include high osmotic pressure chromatography[1−3] to separate polydisperse polymers by their molecular weights and phase fluctuation chromatography[4] to separate copolymers by their chemical compositions. The former utilizes the high osmotic pressure of the semidilute polymer solution to induce the segregation of polymer chains by molecular weight between the confined space and the surrounding bulk solution. Earlier we employed lattice Monte Carlo simulations to investigate the partitioning of monodisperse polymer chains into a slit over a wide range of concentrations.[5] The partition coefficient, defined as the ratio of the concentration in the slit to the one in the bulk solution, was found to increase at high concentrations for different chain lengths and slit widths. It was also found that partitioning at high concentrations is governed by the ratio of the correlation length to the slit width, just as partitioning at low concentrations is governed by the ratio of the radius of gyration to the slit width. However, we did not examine the thermodynamic and statistical properties of the polymer chains in the confined solutions.

Many studies of the thermodynamics of bulk solutions over a wide range of concentrations have been carried out. These studies have given a relatively clear physical picture.[6−11] The osmotic pressure Π of the polymer solution increases with increasing volume fraction ϕ of polymer and obeys $\Pi \sim \phi^{9/4}$ in the semidilute region. The radius of gyration of the chain, R_g, decreases according to $R_g \sim \phi^{-1/8}$. Ohta and Oono[7,8] applied renormalization group theory to the bulk solution and obtained approximate equations for Π and R_g:

$$\frac{\Pi}{\Pi_{\text{ideal}}} = P(X) \equiv 1 + \frac{X}{2}\exp\{[1/X + (1 - 1/X^2)\ln(X + 1)]/4\} \quad (1)$$

$$\frac{R_g}{R_{g0}} = \exp\left\{\frac{1}{16}X\left[\frac{3}{Y} - \left(\frac{3}{2Y^2} + \frac{1}{Y}\right)(\gamma + \ln 2Y) + e^{2Y}\text{Ei}(-2Y)\left(1 - \frac{2}{Y} + \frac{3}{2Y^2}\right)\right]\right\} \quad (2)$$

where Π_{ideal} is the osmotic pressure of the ideal solution at the same concentration, $X = \alpha_c\phi/\phi^*$, ϕ^* is the overlap concentration, $\alpha_c \cong 3.49$, $Y = 1 + X$, $\gamma \cong 0.5772$, and R_{g0} is the value of R_g at dilute limit. These equations are exact up to the order of $4 - d$, where d is the dimensionality. In fact, the equation for Π when $d = 3$ agrees with the scaling law predictions when $X \gg 1$. The equation for R_g, however, does not yield the correct power-law exponent predicted by the scaling law when $d = 3$.

Polymer solutions confined in slits or in tubes have also been studied using various theoretical approaches. The physical picture that emerges is rather complex.[12−22] No counterparts to eqs 1 and 2 have been presented for Π and R_g of the confined solutions. Daoud and de Gennes[12] used the scaling theory to analyze the thermodynamics for a solution of chains (monomer size = a, length = N) confined to a slit of width D. Their theoretical analysis can be summarized in the diagram shown in Figure 1 that depicts the various regimes of the solution confined in a slit. In the diagram, $x = 2R_{g0}/D$ denotes the confinement strength, and $y = R_{g0}/\xi$ is a measure of the concentration where ξ is the correlation length in the bulk solution. They discussed

10.1021/ma991856v CCC: $19.00
Published on Web 04/10/2000

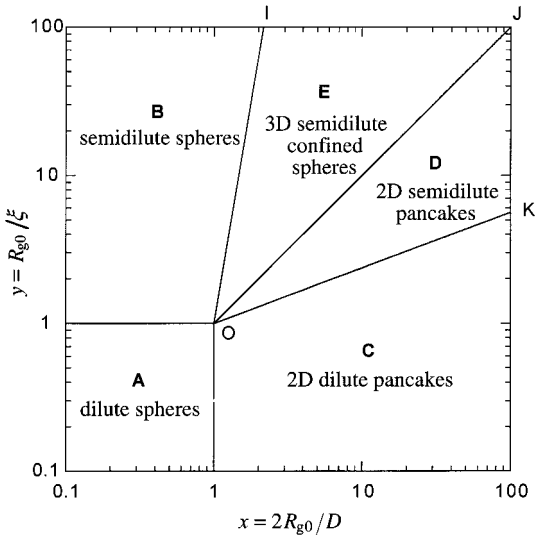

Figure 1. Diagram for polymer solutions confined between two parallel plates.

properties in each region and the crossover between different regions. Their results are summarized below.

Region A: dilute spheres. The radius of gyration of the chains is given by $R_{3g0} = N^{3/5}a$.

Region B: semidilute 3D spheres. The overlap concentration is $\phi_3^* = N^{-4/5}$. The correlation length is $\xi_3(\phi) = a\phi^{-3/4}$. The polymer chains are contracted, and their radii of gyration are given by $R_{3g}(\phi) = R_{3g0}(\phi/\phi^*)^{-1/8} = N^{1/2}a\phi^{-1/8}$.

Region C: dilute 2D pancakes. The radius of gyration of the chains is $R_{2g0} = R_{3g0}(R_{3g0}/D)^{1/4}$.

Region D: semidilute 2D pancakes. The overlap concentration is $\phi_2^* = N^{-1/2}(a/D)^{1/2}$. The correlation length is $\xi_2(\phi) = a(a/D)\phi^{-3/2}$, and the radii of gyration of the chains are $R_{2g}(\phi) = N^{1/2}a(a/D)^{1/2}\phi^{-1/2}$.

Region E: semidilute 3D confined solution. The scaling results are the same as those in region B.

Line OI: crossover from the semidilute 3D solution to the semidilute 3D confined solution. The condition is $R_{3g}(\phi) = D$, which gives $y = x^6$.

Line OJ: crossover from the semidilute 3D confined solution to the semidilute 2D confined solution. The condition is $\xi_3(\phi) = \xi_2(\phi) = D$, which gives $y = x$.

Line OK: crossover from the semidilute 2D confined solution to the dilute 2D confined solution. The condition is $\phi = \phi_2^*$, which gives $y = x^{3/8}$.

The above results are for solutions confined between two parallel plates. Similar scaling results have been obtained for solutions confined by a cylindrical pore. Recently, Lal et al.[18] studied the dimension of polymer chains in Vycor, a porous silica with a typical pore size of 70 Å, by small-angle neutron scattering. They found that the radii of gyration of confined chains are smaller than they are in the bulk solution. They discussed the results in light of the theoretical predictions by Daoud and de Gennes for chains confined in cylindrical pores.[12] The range of polymer concentrations and confinement strengths explored were, however, limited because of experimental restrictions.

In this report, we examine the chemical potential and the dimension of polymer chains in solutions confined between two parallel plates using lattice Monte Carlo simulations for a wide range of conditions. Our aim is to study the thermodynamics of confined solutions in all regions of concentration and confinement strength and compare the results with the theoretical predictions by Daoud and de Gennes.

Table 1. Polymer Chains Used in the Simulations

N	R_{g0}	ϕ^*	N	R_{g0}	ϕ^*
25	2.760	0.341 2	200	9.807	0.070 58
100	6.524	0.116 4	300	12.455	0.052 47
150	8.217	0.088 97	400	14.726	0.042 54

Simulation Method

A regular canonical ensemble simulation was used to calculate the statistical properties such as the chain dimensions. The simulation box is tetragonal with dimensions of $L_x \times L_y \times L_z$ ($L_x = L_y$). There are two solid walls at $z = 1$ and $z = L_z$, extending in the x and y directions. Sites on the layers between them ($L_z - 2$ layers) can be occupied by the beads of polymer chains of a uniform length N. The two walls are purely repulsive due to the excluded-volume interaction. The slit width D is then given as $D = L_z - 1$. Periodic boundary conditions (PBC) are applied in the x and y directions. Chains are equilibrated with the reptation move.[24] After equilibration, the radius of gyration, the chemical potential, and the single chain structure factor of chains are evaluated. The chemical potential is evaluated using the chain insertion method described below.

The chain insertion method is an extension of Widom's particle insertion method.[25] A biased insertion method[26] is used here to increase the success rate for the insertion of a test chain of the same length into a solution at monomer concentration ϕ. Prior to growing the ith segment of the test chain, the number of the empty sites available, z_i, is calculated, and one of those sites is selected randomly. The newly grown segment is given a Rosenbluth weighting factor w_i, defined as $w_i = z_i/(Z - 1)$, where $Z = 6$ is the lattice coordinate. The chemical potential μ of the test chain of length N is calculated with reference to $\mu_{id,NRRW}$, the chemical potential of an ideal nonreverse random walk (monomer overlap is allowed) of the same length on the unconfined lattice at the same ϕ. The difference $\delta\mu$ between μ and $\mu_{id,NRRW}$ is given by

$$\delta\mu/k_BT = (\mu - \mu_{id,NRRW})/k_BT = -\ln\langle(1 - \phi)\prod_{i=2}^{N} w_i\rangle \quad (3)$$

where k_B is the Boltzmann constant, T is the absolute temperature, and $1 - \phi$ accounts for the insertion probability of the first segment. The chain insertion method was successful in the range of concentrations and confinement strengths studied except for a few cases with high concentrations and strong confinement.

Results and Discussion

(A) Bulk Solution. We first show the results of the chemical potentials and the chain contraction factors obtained in the simulation on bulk solutions (regions A and B in Figure 1). Analytical or empirical formulas for the chemical potentials and the chain contraction factors are needed to estimate the partition coefficient of the chains with a pore. The results will also be compared with those for the confined solutions. Table 1 lists the characteristics of the chains used in the simulations. The root-mean-square radii of gyration, R_{g0}, were obtained in the dilute solution limit. The overlap

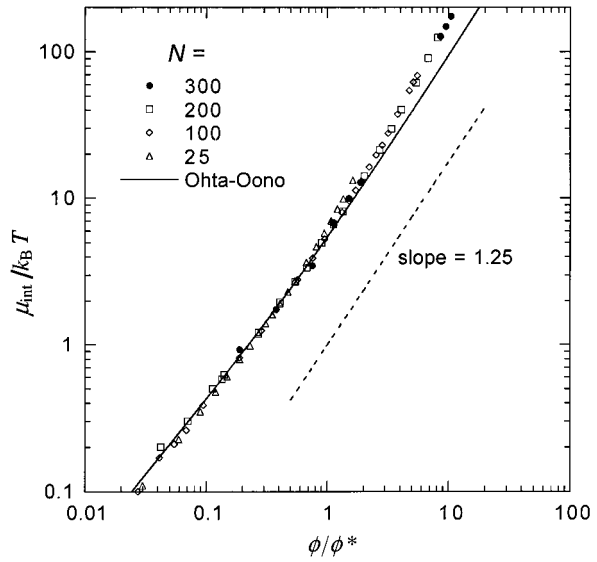

Figure 2. Interaction part of the chemical potential, μ_{int}, in bulk solutions for chain lengths of $N = 25$, 100, 200, and 300, plotted as a function of ϕ/ϕ^*. The Ohta−Oono formula is given by the solid line.

concentration ϕ^* was estimated from $(\phi^*/N)[2^{1/2}(R_{g0} + \alpha)]^3 = 1$, where α accounts for the thickness of a coating needed to translate the R_{g0}^3 calculated on the lattice into the "volume" occupied by the chain in the continuous space. This correction is necessary because, if two monomers are separated by a lattice constant, they are in close contact. Here we want the coating to increase R_0 by a half of the lattice constant. Since[10] $R_{g0}/R_0 = (0.952/6)^{1/2} = 0.398$, we choose $\alpha = 0.199$.

We determined the dependence of $\delta\mu(\phi)$ on ϕ for chains of different lengths ($N = 25$, 100, 200, and 300) in bulk solutions. The range of ϕ examined was from dilute to semidilute and concentrated regions. In the bulk solution, $\delta\mu(\phi) - \delta\mu(0) = \mu_{int}(\phi)$ is due to the interactions only. Symbols in Figure 2 are $\mu_{int}(\phi)$ obtained in the insertion method, plotted as a function of ϕ/ϕ^*. The solid line indicates $\mu_{int}(\phi)$ calculated by

$$\mu_{int}(\phi)/k_BT = P(\phi) - 1 + \int_0^{\phi}[P(\varphi) - 1]\varphi^{-1}\,d\varphi \quad (4)$$

where the Ohta−Oono formula for the compressibility factor $P(\phi) = \Pi/\Pi_{ideal}$ given by eq 1 was used. We first note that nearly all the simulation data fall on a master curve. Second, the scaling law predicts that $\mu_{int} \sim \phi^{1.25}$ in the semidilute region. The entire data presented in Figure 2 do not fit into a straight line, but a good portion of the data show an exponent of 1.25. Third, we see that the agreement between the simulation data and the calculation based on the Ohta−Oono formula is good in the dilute and semidilute regimes ($\phi/\phi^* < 3$). At high concentrations in the so-called concentrated regime, the formula underestimates the increase in the chemical potential, especially for the short chains.

The chain contraction factor, R_g/R_{g0}, in the bulk solution is plotted in Figure 3 as a function of ϕ/ϕ^* for chains with $N = 100$, 150, 200, and 300. Also shown by a dashed line is the calculation based on the formula in eq 2. The simulation results for different chain lengths collapse onto a master curve (solid line), which is approximated by the following empirical formula

$$R_g/R_{g0} = [1 + r_1(\phi/\phi^*) + r_2(\phi/\phi^*)^2]^{-1/16} \quad (5)$$

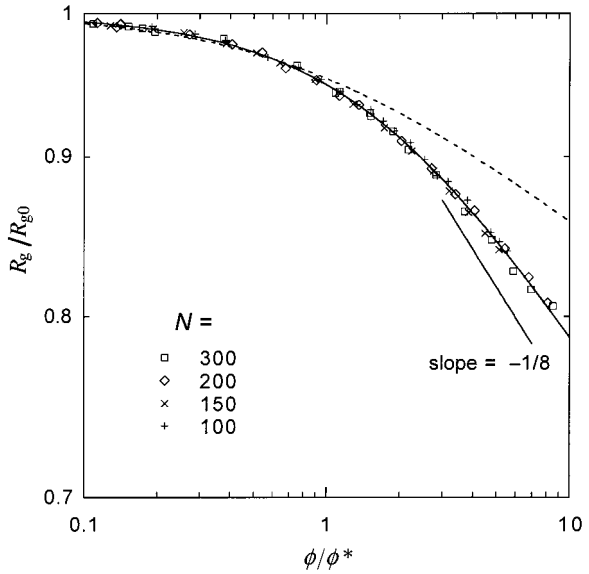

Figure 3. Chain contraction factor, R_g/R_{g0}, in bulk solutions for chain lengths of $N = 100$, 150, 200, and 300, plotted as a function of ϕ/ϕ^*. A dashed line represents the Ohta−Oono formula. The solid line represents the best fit by an empirical formula (see text).

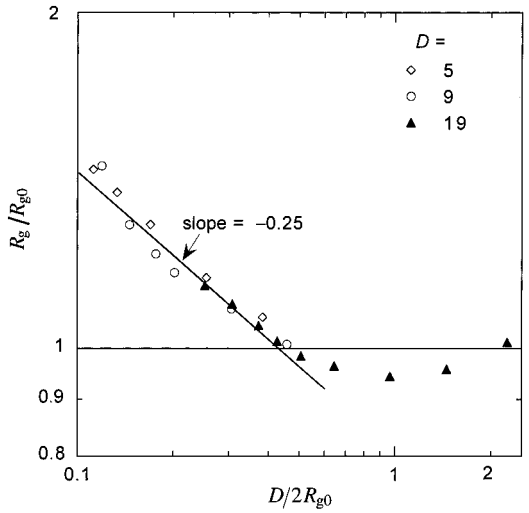

Figure 4. Radius of gyration of chains R_g in the dilute solution limit confined to a slit width of D, reduced by the R_{g0} in the bulk solution, plotted as a function of the reciprocal of the confinement strength, $2R_{g0}/D$. The straight line has a slope of −0.25.

with $r_1 = 0.964\,03$ and $r_2 = 0.348\,90$. The high concentration asymptote of this empirical formula agrees with the scaling theory, namely $R_g(\phi) \sim \phi^{-1/8}$. However, the scaling exponent is achieved only at rather high concentrations, $\phi > 3\phi^*$. In contrast, the Ohta−Oono formula in eq 2 underestimates the chain contractions at high concentrations as noted by Ohta and Ohno.[27]

(B) Confined Solutions at Infinite Dilution. Figure 4 shows a plot of R_g/R_{g0} vs $D/2R_{g0}$ where R_g is the radius of gyration of the chains in the dilute solution limit confined in a slit of width D. Features exhibited in Figure 4 are in agreement with the simulation results reported by van Vliet et al.[28] and can be divided into three regions.

I. For $D/2R_{g0} > 2$, chains do not experience the confinement, and they adopt a 3D conformation. R_g is close to the bulk R_{g0} value.

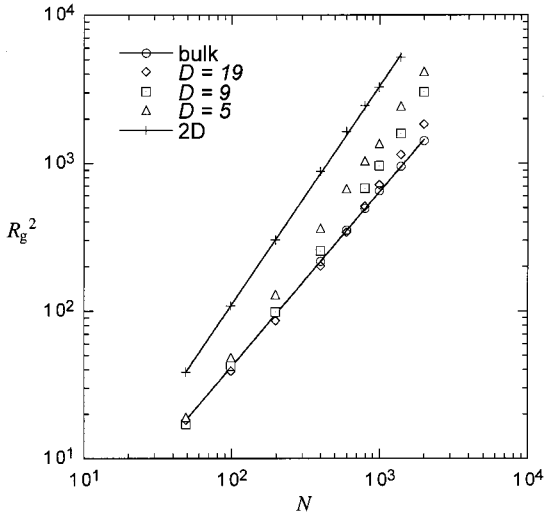

Figure 5. Square radius of gyration, R_g^2, for chains in the dilute solution limit, plotted as a function of the chain length N in bulk, in a 2D solution, and in solutions confined to slits of different widths D.

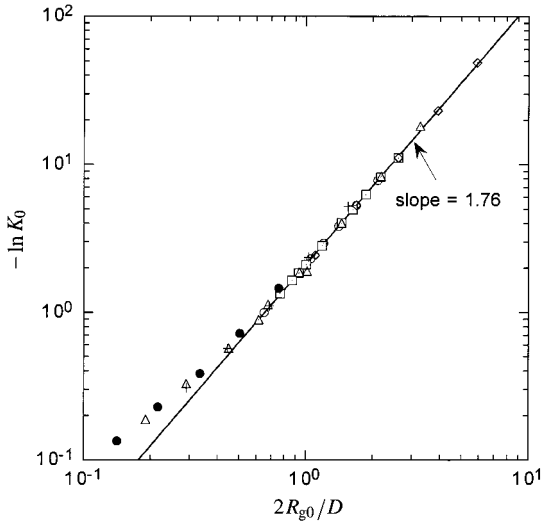

Figure 6. Confinement entropy, $-\ln K_0$, plotted as a function of $2R_{g0}/D$. Data were obtained either by fixing the chain length N and varying D between 4 and 20 or by fixing D and varying N between 25 and 400.

II. For $0.5 < D/2R_{g0} < 2$, R_g is slightly smaller than the bulk R_{g0}. The chains are compressed in the direction perpendicular to the slit walls.

III. When $D/2R_{g0} < 0.5$, R_g is greater than the bulk R_{g0} and $R_g \sim R_{g0}(R_{g0}/D)^{1/4}$. Compression by the walls leads to the elongation along the slit walls.

As the confinement strength increases ($D/2R_{g0}$ decreases), the chains change from 3D nonconfined spheres (region I), to 3D confined spheres (region II), to 2D pancakes (region III). The existence of the middle region in the dilute solution limit was not noted by Daoud and de Gennes. The existence is important to understand the behavior of the confined nondilute solution as shown later.

Figure 5 shows another way to look at the same set of data. The R_g^2 in the dilute solution limit is plotted as a function of N for chains in confined solutions and in bulk. For the latter, we observe the well-known behavior $R_g^2 \sim N^{2\nu_{3D}}$, where $\nu_{3D} = 0.59$. A true 2D solution is achieved in our simulation model when $L_z = 3$ (only one layer can be occupied by the beads of confined chains). In such a true 2D solution, we observe $R_g^2 \sim N^{2\nu_{2D}}$, where $\nu_{2D} = 0.74$, as predicted by the scaling theory. For confined solutions, the dependence of R_g^2 on N is between the two limits and varies with N. When N is small and R_{g0} does not exceed D, the dependence of R_g^2 on N follows that of the bulk solution. As N increases and R_{g0} exceeds D, the dependence of R_g^2 on N follows that of the true 2D solution.

Figure 6 presents $\delta\mu_{conf} - \delta\mu_{bulk} = -\ln K_0$ vs $2R_{g0}/D$, where $\delta\mu_{conf}$ and $\delta\mu_{bulk}$ are the chemical potentials of the chains in confined solution and in bulk at the dilute solution limit, respectively, and K_0 is the partition coefficient of the chains at infinite dilution. Data with $2R_{g0}/D \geq 1$ exhibit a power-law: $-\ln K_0 \sim (2R_{g0}/D)^{1.76}$. The theoretically predicted exponent is $1/\nu_{3D} = 1.69$, slightly smaller than the value observed in the simulation. The deviation in the exponent may be caused by the decrease in the chain dimension at a moderate confinement strength around $2R_{g0}/D \cong 1$. When the chain size decreases, it becomes easier to penetrate the pore, thus rendering a smaller $-\ln K_0$ at $2R_{g0}/D \cong 1$. Note also in the figure that at even smaller $2R_{g0}/D$, the partition coefficients for different chain lengths still fall on a master curve, but the data deviate from the power-law dependence. This deviation is expected, since at large D, $-\ln K_0$ should approach zero as the chains no longer feel the confinement. One can see that the deviation occurs at roughly $2R_{g0}/D \simeq 0.5$, when the dimension of the confined chain approaches the value in the bulk solution.

Table 2. Values of $x = 2R_{g0}/D$

D	$N = 100$	$N = 200$
5	2.63	N/A
9	1.45	2.18
19	0.69	1.03

(C) Confined Nondilute Solutions. We now show the results for nondilute polymer solutions confined to a slit. Master curves such as those presented in Figures 2 and 3 for bulk solutions can no longer be obtained for the confined solutions. Instead, the solutions will exhibit different characteristics depending on the value of $x = 2R_{g0}/D$. If $x < 1$, the solution will show a crossover from dilute 3D spheres to semidilute 3D spheres. If $x > 1$, the solution will show a crossover from dilute 2D pancakes, to 2D semidilute pancakes, and finally to 3D semidilute confined spheres. The chain lengths studied are $N = 100$ in the slits of $D = 5$, 9, and 19 and $N = 200$ in the slits of $D = 9$ and 19. The values of $x = 2R_{g0}/D$ are shown in Table 2.

Figure 7 shows $\delta\mu(\phi)$ for chains with $N = 100$ in a solution confined to a slit of different widths ($D = 5$ and 9) and in a bulk solution. The $\delta\mu(\phi)$ in the $\phi \rightarrow 0$ limit shows the confinement effect on a single chain. The narrower the slit width, the larger the $\delta\mu(0)$. As ϕ increases, $\delta\mu(\phi)$ increases almost at the same pace for different slit widths except for $D = 5$ at low concentrations. When $\mu_{int}(\phi) = \delta\mu(\phi) - \delta\mu(0)$ is plotted as a function of ϕ (not shown), the data for different slit widths nearly overlap with the data for the bulk solution. Similar results are obtained for $N = 200$. We had expected that $\mu_{int}(\phi)$ would be different between the bulk and the confined 2D-like solution, at least for the narrowest slit width. The expectation is based on the known results that the osmotic pressure Π in a 3D solution scales as $\Pi \sim \phi^{9/4}$, while in a 2D solution $\Pi \sim \phi^3$. Therefore, the dependence of $\mu_{int}(\phi)$ on ϕ should show

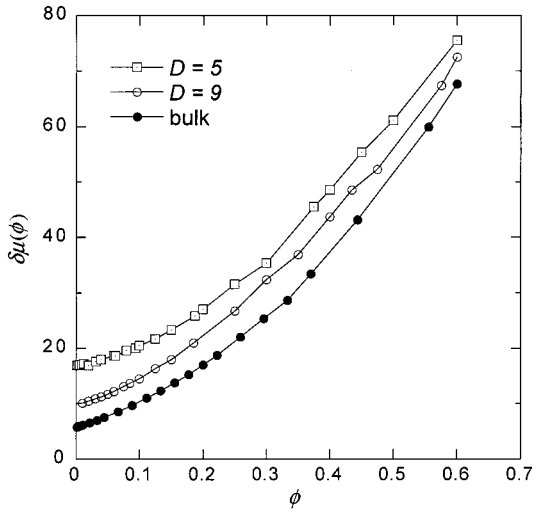

Figure 7. Chemical potential, $\delta\mu(\phi)$, of a chain with $N = 100$ in a solution of chains of the same length confined to a slit of width $D = 5$, 9 and in a bulk solution.

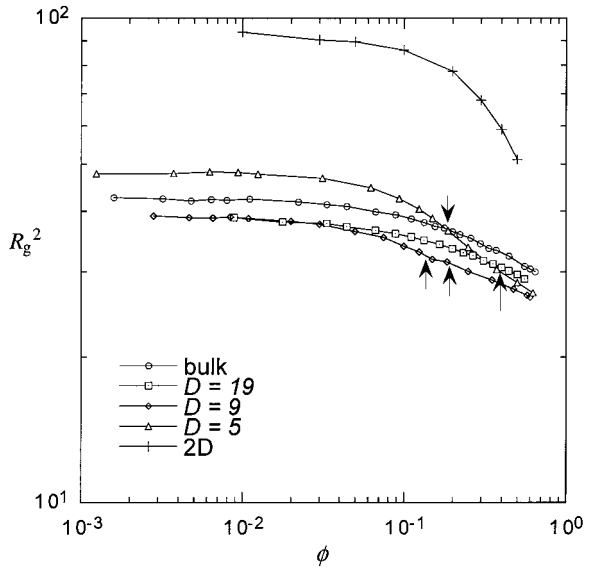

Figure 8. Square radius of gyration, R_g^2, for confined chains with $N = 100$ as a function of ϕ in a slit of width $D = 5$, 9, 19 and in a bulk solution and a true 2D solution. The data for the 2D solution are shifted down by a factor of 0.85.

a characteristic transition from a 3D bulk solution to a 2D-like confined solution with increasing confinement strength. The data suggest that such difference is small and, if any, cannot be detected within the accuracy of our simulations.

In contrast, the chain dimension R_g exhibits the transition characteristics. Figure 8 presents the dependence of $R_g^2(\phi)$ on ϕ for chains with $N = 100$ in slits of different widths, in bulk, and in a true 2D solution. A drastic difference is observed between the results for the narrowest slit ($D = 5$) and those for the wider slits ($D = 9$ and 19). In the dilute solution limit, R_g^2 is almost the same for $D = 9$ and 19 and both are smaller than the counterpart in the bulk solution, but R_g^2 for $D = 5$ is greater than the bulk value. As we have discussed in the preceding section, these results are due to the counteracting effects of the compression in the direction perpendicular to the walls and the elongation along the walls. As ϕ increases, $R_g^2(\phi)$ of confined chains in $D = 19$ and 9 remains smaller than $R_g^2(\phi)$ in the bulk solution. When $D = 5$, in contrast, the confined chains,

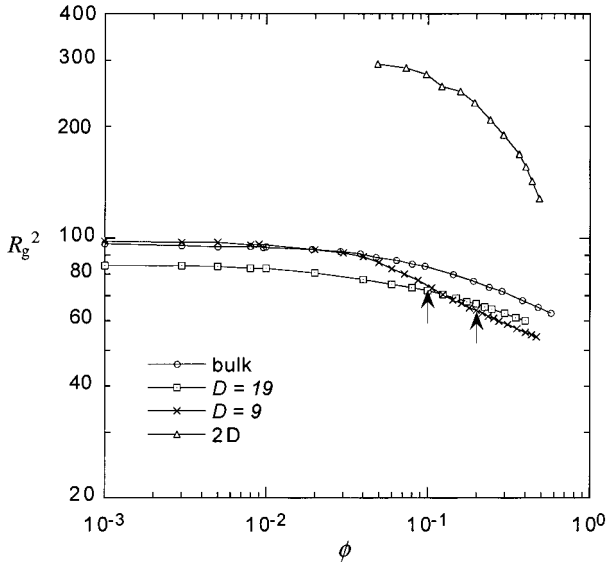

Figure 9. Square radius of gyration, R_g^2, for confined chains with $N = 200$ as a function of ϕ in a slit of width $D = 9$ and 19 and in a bulk solution and a true 2D solution (the data for the 2D solution are not shifted).

although elongated at $\phi = 0$, contract at a much faster pace than the chains in the bulk solution, and $R_g^2(\phi)$ falls below that of the bulk and $D = 19$ at high concentrations. When $R_g^2(\phi)$ is normalized by the $R_g^2(0)$ in the dilute solution limit, the plots for $D = 19$ and the bulk solution become indistinguishable (not shown). In contrast, the plots for $D = 5$ and 9 deviate from the plot for the bulk solution.

A closer inspection of the data for $D = 5$ and $D = 9$ reveals a crossover from a 2D dilute solution to a 2D semidilute solution and finally to a 3D semidilute confined solution (crossovers at line OK and OJ in Figure 1). The arrows in the figure indicate the estimated crossing points with line OK and OJ for $D = 5$ and $D = 9$, where $\xi = R_{g0}(\phi/\phi^*)^{-3/4}$ was used for the estimation. For comparison, the $R_g^2(\phi)$ in a true 2D solution is also shown in the figure. The chain contraction in the 2D solution is much faster than it is in the 3D. The curvature of the plots for $D = 5$ and 9 between the two crossing points is the opposite to the curvature in the other parts of the plot. The trend is more pronounced for $D = 5$ than it is for $D = 9$. The change in the curvature occurs because, as ϕ increases, the chain contraction characteristics show a transition from a rapid decrease in a 2D-like solution to a slow decrease in a 3D-like solution.

The crossover from the 2D confined semidilute solution to the 3D confined semidilute solution can be more clearly seen in Figure 9 which shows $R_g^2(\phi)$ for $N = 200$ in $D = 9$, 19, and in the bulk solution as well as in a true 2D solution. For $D = 19$, the chain contraction follows that of the bulk solution. The two arrows on the plot for $D = 9$ indicate the estimated crossing points with line OK and OJ. The trend similar to the one observed for $N = 100$ in $D = 5$ and 9 in Figure 8 is seen here.

Figure 10 shows the anisotropic chain dimensions for the same set of data in Figure 8, where R_{gxy}^2 and R_{gz}^2 are the mean-square radii of gyration parallel and perpendicular to the slit walls, respectively. In the bulk solution, R_{gz}^2 is half of R_{gxy}^2 for all concentrations. In confined solutions, R_{gxy}^2/R_{gz}^2 depends on ϕ. For $D = 19$, 9, and 5, R_{gxy}^2/R_{gz}^2 is 3.6, 11.7, and 39.6, respectively,

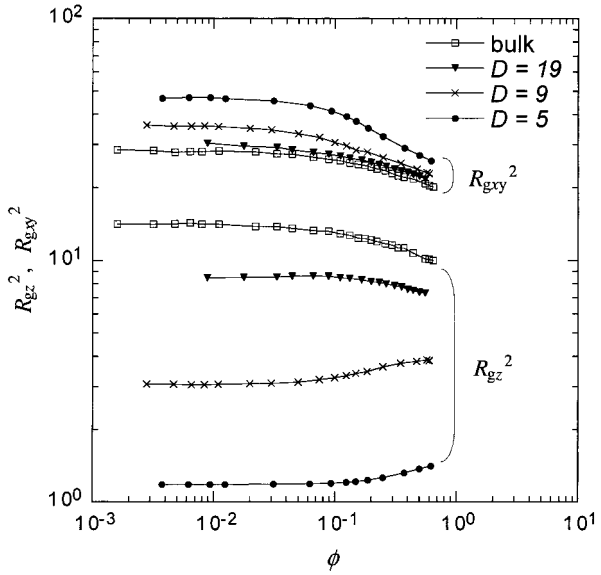

Figure 10. Individual components in the radius of gyration of confined chains, R_{gxy}^2 and R_{gz}^2, plotted as a function of ϕ for $N = 100$ in a slit of widths $D = 5$, 9, and 19 and in a bulk solution.

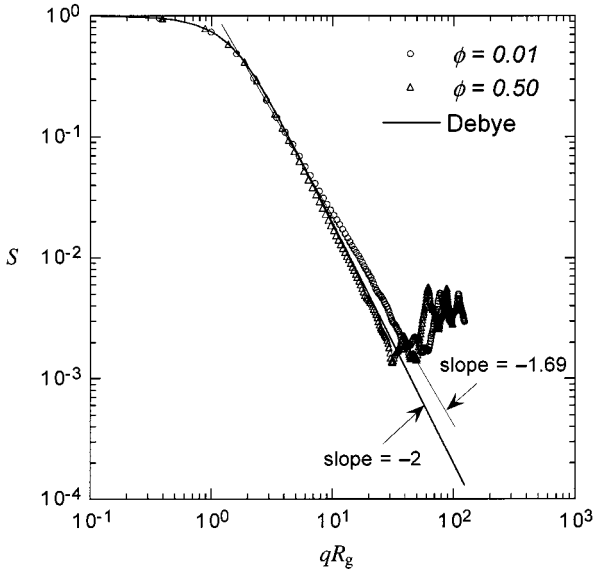

Figure 11. Single chain structure factors for chains with $N = 300$ in a bulk solution at $\phi = 0.05$ and 0.5, plotted as a function of qR_g.

in the dilute solution limit. The confined chains exhibit a more pronounced pancake shape as the slit narrows. As ϕ increases, shielding of the excluded-volume interaction causes R_{gxy}^2 to decrease in all slit widths. The change in R_{gz}^2, however, depends on the slit width and is controlled by two opposing factors. One factor is related to the density profile. At low concentrations, polymer segments are strongly repelled by the slit wall, producing a thick depletion layer. As ϕ increases, repulsion between polymer segments pushes them closer to the wall, resulting in a thinner depletion layer and a larger R_{gz}^2. The other factor is related to the shielding of the excluded-volume interaction that causes the chain to contract. When the correlation length in the confined solution is smaller than the slit width, the further shielding of the excluded-volume interaction at high concentration causes not only R_{gxy}^2 to continue to decrease, but R_{gz}^2 to decrease as well. The first factor dominates in the narrower slits such as $D = 5$ and 9. The second factor dominates in the wider slits such as $D = 19$.

(D) Single Chain Structure Factor. Finally we present the single chain structure factor $S(q)$ in the confined solution. Figure 11 shows $S(q)$ for $N = 300$ in the bulk at two concentrations, $\phi = 0.01$ and 0.50. The $S(q)$ is plotted as a function of qR_g where q is the scattering vector and R_g is the radius of gyration at the given concentration. In the dilute solution limit, the structure factors for different chain lengths, when plotted as a function of qR_g, overlap with each other. At high concentrations, the structure factors for different chain lengths also overlap when the concentrations are close to each other. Also included in the plot is the Debye function for the single chain structure factor. The exponent in the high q range (not including the portions that fluctuate) is indicated for each plot. In the dilute solutions, when there is excluded-volume interactions, $S(q)$ scales as $S(q) \sim q^{-1/\nu_{3D}} = q^{-1.69}$. In the semidilute solution, chains are ideal on scales greater than ξ, the correlation length. Therefore, when $q\xi < 1$, $S(q)$ follows the Debye function and $S(q) \sim q^{-2}$. Similar results have been reported by Paul et al.[29]

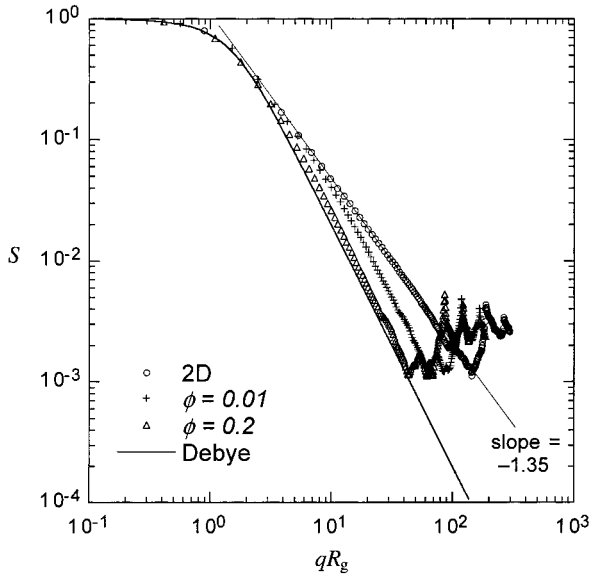

Figure 12. Single chain structure factors for chains with $N = 400$ confined to a slit of width $D = 5$ at two concentrations, $\phi = 0.01$, $\phi = 0.2$, with the Debye function shown by the solid line and the structure factor in a 2D solution in the dilute solution limit.

The single chain structure factor in a weakly confined solution does not show much difference from the counterpart in a 3D bulk solution. A difference is only seen in a strongly confined solution in the dilute solution limit. Figure 12 compares the single chain structure factor for $N = 400$ in $D = 5$ ($x = 2R_{g0}/D = 5.9$) at two different concentrations with the $S(q)$ in a true 2D solution at the dilute solution limit and the Debye function. In the dilute 2D solution, we observe the expected scaling result, $S(q) \sim q^{-1.35}$ ($1/\nu_{2D} = 1.35$). In $D = 5$ at $\phi = 0.01$, the chains are strongly confined and elongated along the slit walls. The $S(q)$ in $D = 5$ at $\phi = 0.01$ follows the structure factor in the 2D solution at low q, but deviates at high q, rather adopting an exponent close to that of the 3D bulk solution. The transition occurs approximately at a distance equal to the slit width ($qD \sim 2\pi$). Thus, $S(q)$ possesses 2D characteristics on a distance greater than D and 3D

characteristics on a distance smaller than D. At $\phi = 0.2$ in $D = 5$, the chains are still of 2D pancake shapes, but the solution is in the 2D semidilute region and the excluded-volume interaction is partially shielded. The structure factor is now close to the Debye function. At even higher concentrations, $S(q)$ in $D = 5$ follows the Debye function more closely. This indicates that when the excluded-volume interaction is shielded, the single chain structure factor approaches the Debye function for both the 2D-like confined solution and the 3D-like confined solution. In a true 2D solution, however, $S(q)$ does not approach the Debye function even at $\phi = 0.5$ (not shown). This difference is probably due to the difficulty to shield the excluded-volume interactions in a true 2D solution.

Conclusions

We have used lattice Monte Carlo simulations to examine the thermodynamic properties of solutions confined between two parallel plates in a wide range of concentrations and slit widths. In the bulk solution, we have observed $\delta\mu_{\text{int}} \sim (\phi/\phi^*)^{1.25}$ and $R_g/R_{g0} \sim (\phi/\phi^*)^{-1/8}$, as predicted by the scaling-law theory. The latter scaling exponent is, however, only observed at $\phi/\phi^* \geq 3$. The dependence of $\delta\mu_{\text{int}}$ on ϕ does not show any detectable difference between the confined solutions and the bulk solutions. In contrast, the dependence of R_g on ϕ shows a clear difference between a bulk solution and a strongly confined solution. At strong confinement ($x = 2R_{g0}/D > 2$), R_g of the confined chains at low concentrations is larger than R_g of the bulk solution. At high concentrations, however, R_g of the confined chains becomes smaller than R_g of bulk solution. The transition of a confined solution from a 2D semidilute solution to a 3D semidilute solution with increasing ϕ is thus observed. The transition is characterized by the change in the curvature in the plot of R_g as a function of ϕ. The single chain structure factor, $S(q)$, in a strongly confined solution at the dilute solution limit exhibits the features of a bulk solution at a length scale smaller than the slit width and the features of a true 2D solution at a length scale greater than the slit width. At high concentrations when the excluded-volume interaction is shielded, the $S(q)$ for the confined 2D-like solution and the confined 3D-like solution both approach the Debye function.

Acknowledgment. This research is supported by the National Science Foundation (DMR-9876360) and the Petroleum Research Fund (PRF-32707-GB5), administered by the American Chemical Society. We also acknowledge the computer resource support provided by the North Carolina Super Computer Center.

References and Notes

(1) Luo, M.; Teraoka, I. *Macromolecules* **1996**, *29*, 4226.
(2) Luo, M.; Teraoka, I. *Polymer* **1998**, *39*, 891.
(3) Teraoka, I.; Luo, M. *Trends Polym. Sci.* **1997**, *5*, 528.
(4) Xu, Y.; Teraoka, I. *Macromolecules* **1998**, *31*, 4143.
(5) Wang, Y.; Teraoka, I. *Macromolecules* **1997**, *30*, 8473.
(6) Casassa, E. F. *J. Polym. Sci., Polym. Lett. Ed.* **1967**, *5*, 773.
(7) de Gennes, P. G. *Scaling Concepts in Polymer Physics*; Cornell University Press: Ithaca, NY, 1979.
(8) Oono, Y.; Ohta, T.; Freed, K. F. *J. Chem. Phys.* **1981**, *74*, 6458.
(9) Ohta, T.; Oono, Y. *Phys. Lett.* **1982**, *89A*, 460.
(10) des Cloizeaux, J. *J. Phys.* (*Paris*) **1975**, *36*, 281.
(11) des Cloizeaux, J.; Jannik, G. *Polymers in Solution: Their Modeling and Structure;* Clarendon: Oxford, 1990.
(12) Daoud, M.; et al. *Macromolecules* **1975**, *8*, 804.
(13) Daoud, M.; De Gennes, P. G. *J. Phys.* (*Paris*) **1977**, *38*, 85.
(14) Daoudi, S.; Brochard, F. *Macromolecules* **1978**, *11*, 751.
(15) Kremer, K.; Binder, K. *J. Chem. Phys.* **1984**, *81*, 6381.
(16) Nemirovsky, A. M.; Freed, K. F. *J. Chem. Phys.* **1985**, *83*, 4166.
(17) Douglas, J. F.; Nemirovsky, A. M.; Freed, K. F. *Macromolecules* **1986**, *19*, 2041.
(18) Honeycutt, J. D.; Thirumalai, D. *J. Chem. Phys.* **1990**, *90*, 4542.
(19) Brochard-Wyart, F.; Raphael, E. *Macromolecules* **1990**, *23*, 2276.
(20) Raphael, E.; Pincus, P. *J. Phys. II* **1992**, *2*, 1341.
(21) Kierlik, E.; Rosinberg, M. L. *J. Chem. Phys.* **1994**, *100*, 1716.
(22) Thompsom, A. P.; Glandt, E. D. *Macromolecules* **1996**, *29*, 4314.
(23) Lal, J.; Sinha, S. K.; Auvray, L. *J. Phys. II* **1997**, *7*, 1597.
(24) Wall, F. T.; Mandel, F. *J. Chem. Phys.* **1975**, *63*, 4592.
(25) Rosenbluth, M. N.; Rosenbluth, A. W. *J. Chem. Phys.* **1955**, *96*, 2395.
(26) Frenkel, D.; Mooju, G. C. A. M.; Smit, B. *J. Phys.: Condens. Matter* **1992**, *3*, 3053.
(27) Oono, Y. *Adv. Chem. Phys.* **1985**, *61*, 301.
(28) Van Vliet, J. H.; Luyten, M. C.; ten Brinke, G. *Macromolecules* **1992**, *25*, 3802.
(29) Paul, W.; Binder, K.; Heerman, D. W.; Kremer, K. *J. Phys. II* **1991**, *1*, 37.

MA991856V